Hydrodynamic Effects and Receptor Interactions of Platelets and Their Aggregates in Linear Shear Flow

Pushkar Tandon and Scott L. Diamond
Institute for Medicine and Engineering, Department of Chemical Engineering, University of Pennsylvania, Philadelphia, Pennsylvania 19104 USA

ABSTRACT We have modeled platelet aggregation in a linear shear flow by accounting for two body collision hydrodynamics, platelet activation and receptor biology. Considering platelets and their aggregates as unequal-sized spheres with DLVO interactions ($\psi_{platelet} = -15$ mV, Hamaker constant = 10^{-19} J), detailed hydrodynamics provided the flow field around the colliding platelets. Trajectory calculations were performed to obtain the far upstream cross-sectional area and the particle flux through this area provided the collision frequency. Only a fraction of platelets brought together by a shearing fluid flow were held together if successfully bound by fibrinogen cross-bridging GPIIb/IIIa receptors on the platelet surfaces. This fraction was calculated by modeling receptor-mediated aggregation using the formalism of Bell (Bell, G. I. 1979. A theoretical model for adhesion between cells mediated by multivalent ligands. *Cell Biophys.* 1:133–147) where the forward rate of bond formation dictated aggregation during collision and was estimated from the diffusional limited rate of lateral association of receptors multiplied by an effectiveness factor, η, to give an apparent rate. For a value of $\eta = 0.0178$, we calculated the overall efficiency (including both receptor binding and hydrodynamics effects) for equal-sized platelets with 50,000 receptors/platelet to be 0.206 for $G = 41.9\ s^{-1}$, 0.05 for $G = 335\ s^{-1}$, and 0.0086 for $G = 1920\ s^{-1}$, values which are in agreement with efficiencies determined from initial platelet singlet consumption rates in flow through a tube. From our analysis, we predict that bond formation proceeds at a rate of ~0.1925 bonds/μm^2 per ms, which is ~50-fold slower than the diffusion limited rate of association. This value of η is also consistent with a colloidal stability of unactivated platelets at low shear rates. Fibrinogen was calculated to mediate aggregation quite efficiently at low shear rates but not at high shear rates. Although secondary collisions (an orbitlike trajectory) form only a small fraction of the total number of collisions, they become important at high shear rates (>750 s^{-1}), as these are the only collisions that provide enough time to result in successful aggregate formation mediated by fibrinogen. The overall method provides a hydrodynamic and receptor correction of the Smoluchowski collision kernel and gives a first estimate of η for the fibrinogen-GPIIb/IIIa cross-bridging of platelets. We also predict that secondary collisions extend the shear rate range at which fibrinogen can mediate successful aggregation.

Nomenclature

A	mobility function along line of centers of the particles;
A_{coll}	collision area;
a_1, a_2	radii of the colliding particles;
B	mobility function normal to the line of the centers of the colliding particles;
C	correction to Stokes law taking into account presence of second sphere;
C_A	nondimensional attractive force parameter;
C_R	nondimensional repulsion force parameter;
G	shear rate;
F_A	van der Waals attractive force;
F_R	repulsion force;
H_A	Hamaker constant;
K_d	Dissociation constant;
k_f	forward rate of bond formation;
L	ligand (fibrinogen) concentration;
N_i	Number density of aggregates of size class i;
N_b	bonds per unit area;
N_{crit}	critical number of bonds to hold aggregate together;
N_{rec}	number of receptors per unit area;
v	volume;
V	relative velocity between the aggregates;
s	dimensionless distance between the aggregates;
$\beta(i,j)$	collision frequency between particles of size classes i and j;
β_G	Smoluchowski collision frequency;
ϵ	collision efficiency;
ϵ_h	hydrodynamic collision efficiency;
ϵ_{r+h}	overall collision efficiency (including hydrodynamic and receptor effects);
ϵ_m	permittivity of the medium;
ϕ	solid volume fraction;
η	effectiveness factor;
λ	size ratio of the colliding aggregates;
τ	collision time;
ξ	dimensionless separation distance between the colliding aggregates;
$\psi_{platelet}$	platelet potential.

Received for publication 23 April 1997 and in final form 19 August 1997.

Address reprint requests to Scott L. Diamond, Institute for Medicine and Engineering, Department of Chemical Engineering, University of Pennsylvania, 394 Towne Bldg., 220 S. 33rd St., Philadelphia, PA 19104. Tel.: 215-898-8652; Fax: 215-573-2093; E-mail: sld@eniac.seas.upenn.edu.

0006-3495/97/11/2819/17 $2.00

INTRODUCTION

Platelet activation, adhesion, and aggregation play a major role in thrombosis, atherosclerosis, and restenosis after angioplasty. An injury to the vessel wall and exposure of tissue factor and collagen trigger a complex set of reactions

resulting in prothrombin conversion as well as adhesion and activation of platelets. Platelets can be activated by high shear stresses or by agonists (e.g., ADP, thromboxane, thrombin) released or produced as a result of coagulation reactions. The activation of the platelets involves shape change and release of ADP, as well as activation of glycoprotein IIb/IIIa receptors [Frojmovic et al. (1991); Weisel et al. (1992)]. The aggregation of platelets colliding under conditions of fluid flow is mediated through fibrinogen cross-bridging of GPIIb/IIIa and von Willebrand factor (vWF) interactions with GPIb-IX and GPIIb/IIIa.

Platelet membrane glycoproteins IIb and IIIa form a Ca^{2+}-dependent noncovalent complex (GPIIb/IIIa or $\alpha_{IIb}\beta_3$ integrin), which functions as a receptor for fibrinogen. Fibrinogen binds to GPIIb/IIIa in a specific, saturable manner via the dodecapeptide sequence $\gamma_{400-411}$ on the D domain of fibrinogen. On resting platelets, GPIIb/IIIa receptors are maintained in an inactive conformation. However, upon platelet activation, GPIIb/IIIa receptors undergo conformational changes to become competent receptors for soluble fibrinogen and plasma proteins such as vWF. Fibrinogen binds to GPIIb/IIIa receptors (~50,000 binding sites/platelet) with a dissociation constant of $K_d = 0.1$ μM [Bennett and Vilaire (1979); Marguire et al. (1980)].

The shear stress-induced activation of platelets is observed only above shear rates of ~3000 s^{-1} [Huang and Hellums (1993a–c)]. ADP and other agonists can stimulate platelets and induce aggregation even for shear rates as low as 50 s^{-1}. ADP-induced aggregation of platelets in flow through tubes has been studied by Goldsmith and co-workers [Bell et al. (1989a,b; 1990); Goldsmith et al. (1994, 1995)]. In those studies, the agonist-induced aggregation in Poiseuille flow was studied between mean shear rates of 50 to 2000 s^{-1} for the effects of shear rates, donor sex, ADP concentrations, and fibrinogen levels. They also report enhanced aggregation rates in the presence of red blood cells. Red blood cells (RBCs) not only increase the collision frequency because of augmented diffusion, but also enhance platelet aggregation by releasing ADP. Interestingly, RBCs can prolong the mean contact time during collisions in tube flow by ~60% due to complex multiparticle interactions [Goldsmith et al. (1995)].

Hellums and co-workers [Belval and Hellums (1986); Huang and Hellums (1993 a–c)] have applied the population balance equation (PBE) along with the Smoluchowski two-body collision theory to quantify the spatially homogeneous, shear induced-aggregation and disaggregation kinetics of platelets in anticoagulated plasma. The Smoluchowski expression to model the collision frequency assumes that particles are spheres, follow linear trajectories, and collide without hydrodynamic interaction. Only a fraction of the collisions predicted by Smoluchowski theory were considered to result in successful aggregation. This fraction (denoted as ϵ and called the collision efficiency) was an empirical parameter in their study and was obtained by regression of the experimental data and contained all the platelet receptor biology and hydrodynamic effects.

In the present study, we present methods to predict the collision efficiency parameter ϵ [an empirical parameter in the earlier studies of Huang and Hellums (1993a–c) and Bell et al. (1989a,b; 1990)] systematically taking into account effects due to hydrodynamics and receptor interactions. The hydrodynamic effect on the collision frequency is calculated by considering platelets and their aggregates as solid spheres with DLVO interactions and performing trajectory calculations to obtain the far upstream cross-sectional area. Particle flux through this cross-section allows prediction of the particle collision frequency. Particles colliding together by the shear fluid flow are bound together if enough time is available for fibrinogen cross-bridging GPIIb/IIIa receptors on the platelet surface. The successful collision frequency, including both receptor and hydrodynamic effects, has been included in a population balance framework to predict the size evolution of the aggregate population. Predictions have been compared with the experimental data of Bell et al. (1989a,b) and Huang and Hellums (1993). Generalization of these methods to predict aggregation behavior of other cells or more complex binding chemistries may be possible.

THEORY

Size distributions of aggregating platelets in a shear field

The population balance framework has been used to predict the size distributions of platelets undergoing spatially homogeneous, shear-induced aggregation in anticoagulated plasma [Belval and Hellums (1986); Huang and Hellums (1993a–c)]. The PBE [Smoluchowski (1917)] defines the rate of change of number density, N_i, of platelet aggregates comprised of i singlets (platelets) and is given as:

$$\frac{\partial N_i}{\partial t} = \frac{1}{2}\sum_{j=1}^{i-1} \beta(j, i-j) N_j N_{i-j} - N_i \sum_{j=1}^{\infty} \beta(i, j) N_j \qquad (1)$$

where $\beta(i, j)$ is the successful shear-induced collision frequency between aggregates comprised of i and j singlets, respectively. Eq. 1 is the discrete PBE without disaggregation. The first term on the right-hand side (RHS) of Eq. 1 represents the birth of particles with i singlets by aggregation of particles having fewer than i singlets (factor of ½ prevents double counting). The second term of the RHS is associated with the death of particles with i singlets as a result of them aggregating with other particles to form even larger particles. Solution of Eq. 1 (see Appendix) with appropriate initial conditions yields the evolution of aggregate number density distribution with time.

Collision frequency $\beta(u, v)$: hydrodynamic effects

Assuming particles follow linear trajectories in shear flows by neglecting hydrodynamic interactions, Smoluchowski (1917) suggested the following expression for the collision

frequency for two spheres of volume u and v undergoing shear-induced aggregation:

$$\beta_G(u, v) = \frac{G}{\pi}[u^{1/3} + v^{1/3}]^3 \tag{2}$$

where G is the shear rate. Here particle volume represents the sum of the primary particle volumes comprising the aggregate. Belval and Hellums (1986) and Huang and Hellums (1993 a–c) have used Eqs. 1 and 2 to model the platelet population dynamics of heparinized platelet-rich plasma subjected to linear shear field considering only a fraction of the collisions (denoted as collision efficiency ϵ or ϵ_{r+h} in the present study) given by Eq. 2 result in successful collisions leading to aggregation. This empirical parameter ϵ in earlier studies was considered to include both hydrodynamic and receptor effects. However, a detailed hydrodynamics analysis [van de Ven (1989)] reveals that two solid spheres in shear flow will not touch in the absence of any attractive forces (such as van der Waals). Furthermore, the collision efficiency ϵ is dependent on the size ratio of the two aggregates colliding. The efficiency of equal-sized aggregate collisions can be significantly greater than the efficiency for unequal sized particles.

We present methods to systematically predict the collision efficiency ϵ [which was an empirically determined parameter in the studies of Huang and Hellums (1993a–c) and Bell et al. (1989a,b; 1990)] taking into account the interplay of shear flow hydrodynamics and platelet receptor biology and their effect on the evolution of particle size distribution. To include the effects due to these factors on the population dynamics, a modified collision kernel is defined as:

$$\beta = \epsilon_r\epsilon_h\left(\frac{\beta_G}{1-\alpha}\right) = \epsilon_{r+h}\left(\frac{\beta_G}{1-\alpha}\right) \tag{3}$$

where ϵ_h is the hydrodynamic collision efficiency, ϵ_r is the receptor binding efficiency, and β_G is the Smoluchowski expression for the collision frequency given by Eq. 2. The product $\epsilon_h\beta_G$ gives the actual collision frequency considering detailed flow fields around the colliding spherical particles. The hydrodynamic efficiency ϵ_h depends in general on particle size ratios, surface charge and electrostatic repulsion, van der Waals attraction, and the shear rate. ϵ_r represents the fraction of collisions that results in GPIIb/IIIa-fibrinogen binding leading to successful aggregation of the colliding particles. The expression in the denominator on the RHS of Eq. 3 takes into account the fact that the resulting aggregates are porous with void fraction α. However, our present model does not consider the effects of surface roughness or permeable flow through the porous aggregates. Indeed, even in the absence of any attractive forces, there would be a nonzero hydrodynamic collision efficiency between two colliding porous or rough aggregates [Michalopoulou et al. (1991)].

After platelet activation, the rapid shape change of platelets results in a spherical cell with pseudopods [Frojmovic et al. (1991)]. Recently, the hydrodynamics of spiked spheres has been described mathematically [Kim and Karrila (1991)] but their collisions have yet to be characterized. While platelets and their aggregates are rough and nonspherical with pseudopods, hydrodynamics and collisions of such morphologically complex aggregates is not yet completely understood. As a first step to investigate hydrodynamic contributions to aggregation dynamics, we treat platelets and their aggregates as smooth solid spheres following earlier approaches [Huang and Hellums (1993a–c); van de Ven (1989); Adler (1981 a,b); Wang et al. (1994); Zeichner and Schowalter (1977)]. To find the flow field around two spheres in a simple shear field, the creeping flow equations are solved with the no-slip boundary condition at the surface of each sphere and with the velocities approaching the undisturbed flow field at large distances from the spheres. For a spherical coordinate system (r, θ, ϕ) system, the relative trajectory of two spheres of arbitrary radii a_1 and a_2 in a shear field of strength G (see Fig. 1, $V_x = Gy$), can be described by the equations:

$$V_r = \frac{dr}{dt} = Gr[1 - A(r, \lambda)]\sin^2\theta \sin\phi\cos\phi + F_r \tag{4a}$$

$$V_\theta = r\frac{d\theta}{dt} = Gr[1 - B(r, \lambda)]\sin\theta\cos\theta\sin\phi\cos\phi \tag{4b}$$

$$V_\phi = r\sin\theta\frac{d\phi}{dt} = Gr\left(\cos^2\phi - \frac{B(r, \lambda)}{2}\cos 2\phi\right)\sin\theta \tag{4c}$$

where F_r is the effect due to external forces, and $\lambda = a_2/a_1$ ($\lambda \leq 1$). Functions A and B are the mobility functions along lines of centers and normal to the line of centers, respectively, describing the effects of hydrodynamic interactions between the particles [Batchelor and Green (1972)]. In

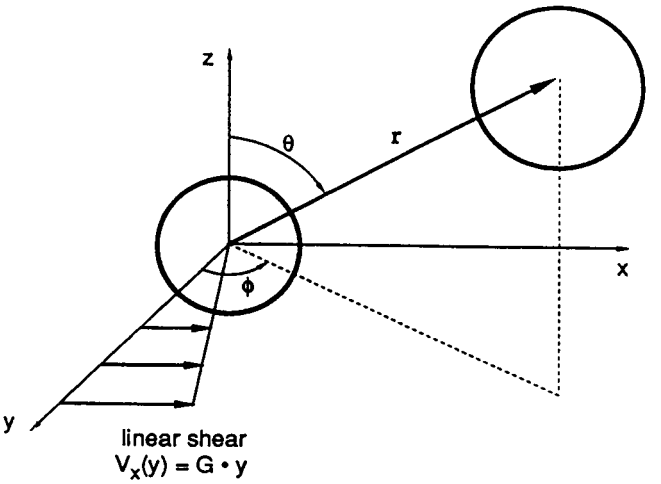

FIGURE 1 Schematic of two unequal sized platelets or aggregates (of radii a_1, and a_2) in a spherical coordinate (r, ϕ, θ) system. The interaction of the particles in a linear shear field given by $V_x = G \cdot y$ where G is the local shear rate of blood flow is treated for van der Waals attraction, and electrostatic repulsion between the particles.

determining the flow field, the interparticle forces of van der Waals attraction and electrostatic repulsion are considered and Eq. 4 is made dimensionless by normalizing distances with the average radius $\bar{a}$ ($= (a_1+a_2)/2$) and time with $1/G$ ($s = r/\bar{a}$, $t^* = Gt$, $\xi = (r - a_1 - a_2)/\bar{a} = s - 2$). The nondimensional equivalent of Eq. 4 is:

$$\frac{ds}{dt^*} = s[1 - A(\xi, \lambda)]\sin^2\theta \sin\phi\cos\phi + \frac{C(\xi, \lambda)(F_A + F_R)}{3\pi\mu a_1^2 G(1 + \lambda)} \quad (5a)$$

$$\frac{d\theta}{dt^*} = [1 - B(\xi, \lambda)]\sin\theta\cos\theta\sin\phi\cos\phi \quad (5b)$$

$$\frac{d\phi}{dt^*} = \cos^2\phi - \frac{B(\xi, \lambda)}{2}\cos 2\phi \quad (5c)$$

In Eq. 5, μ is the plasma viscosity, ξ is the nondimensional gap separation between the particles, F_A is the van der Waals attractive force, F_R is the repulsion force, and $C(\lambda,\xi)$ is the correction to the Stokes law taking into account the presence of the second sphere. For $p = 2\pi\xi\bar{a}/\lambda_L$, the van der Waals and electrostatic forces are defined as [van de Ven (1989)]:

$$\frac{CF_A}{3\pi\mu a_1^2 G(1 + \lambda)} = \frac{-C_A\lambda C}{(1 + \lambda)^4}\left[\frac{1 + 3.54p}{\xi^2(1 + 1.77p)^2}\right] \quad \text{for } p < 1$$

$$\frac{CF_A}{3\pi\mu a_1^2 G(1 + \lambda)} = \frac{-C_A\lambda C}{(1 + \lambda)^4\xi^2}\left[\frac{0.98}{p} - \frac{0.434}{p^2} + \frac{0.0674}{p^3}\right] \quad \text{for } p \geq 1$$

$$\frac{CF_R}{3\pi\mu a_1^2 G(1 + \lambda)} = \frac{C_R\lambda C}{(1 + \lambda)^2}\left[\frac{(\psi_1^2 + \psi_2^2)\exp(-\kappa a_1\xi(1 + \lambda)/2) - 2\psi_1\psi_2}{\psi_{ref}^2\sinh(\kappa a_1\xi(1 + \lambda)/2)}\right] \quad (6)$$

Here $1/\kappa$ is the Debye length, ψ_1 and ψ_2 are potential on each of the spheres, and λ_L is the London wavelength. Nondimensional parameters C_A and C_R are:

$$C_A = \frac{2H}{9\pi G\mu a_1^3} \quad C_R = \frac{\epsilon_m\kappa\psi_{ref}^2}{3\pi\mu G a_1} \quad (7)$$

where H is the Hamaker constant, ϵ_m is the permittivity of the medium, and ψ_{ref} is a reference potential. Behavior of functions $A(\xi, \lambda)$, $B(\xi, \lambda)$, and $C(\xi, \lambda)$ over the spectrum of size ratios and gap separations are needed to integrate Eq. 5 to obtain particle trajectories. We have used the behavior of two unequal-sized particles in a shear flow field in the asymptotic limits of very small separation of $\xi \leq 0.01$ and large separation $\xi \geq 1$ [Batchelor and Green (1972); Adler (1981a)] for generating the complete flow field around the two spheres. At intermediate separations of $0.01 \leq \xi \leq 1$, we developed matching functionals shown in Eqs. 8–10. Results from these correlations are within 2% of the results in the literature [Batchelor and Green (1972), Adler (1981a)] (see Appendix) who used detailed hydrodynamic calculations in the intermediate regime over a range of size ratios (for $\lambda = 0.1$, 0.2, 0.5, and 1.0).

Behavior of $A(\xi, \lambda)$

$\xi \leq 0.01$

$$A(\lambda, \xi) = 1 - K_1(\lambda)\xi(1 + \lambda)/2$$

where $K_1(\lambda) = 0.206 + 19.245\lambda - 27.254\lambda^2 + 11.881\lambda^3$

$\xi \geq 1$

$$A(s) = \frac{20(1 + \lambda^3)}{(1 + \lambda)^3 s^3} - \frac{48[3(1 + \lambda^5) + 5\lambda^2(1 + \lambda)]}{3s^5(1 + \lambda)^5}$$

$0.01 < \xi < 1$

$$A(\xi) = \frac{1}{1 + A_1\xi^{B_1}} \quad (8)$$

A_1 and B_1 are constants determined by matching the values of A at $\xi = 0.01$ and 1.

Behavior of $B(\xi, \lambda)$

$\xi \leq 0.00075$

$$B(\xi, \lambda) = K_2(\lambda) + \frac{K_3(\lambda)}{\log_e\xi + \log_e((1 + \lambda)/2)}$$

where $K_2(\lambda) = 1.141 - 1.446\lambda + 0.709\lambda^2$, and

$$K_3(\lambda) = 0.439 + 12.747\lambda - 31.211\lambda^2 + 18.806\lambda^3$$

$\xi \geq 1$

$$B(\lambda, \xi) = \frac{32[3(1 + \lambda^5) + 5\lambda^2(1 + \lambda)]}{3s^5(1 + \lambda)^5}$$

$0.00075 < \xi < 1$

$$B(\lambda, \xi) = A_2\xi^{0.25} + B_2 \quad (9)$$

A_2 and B_2 are constants determined by matching the values of B at $\xi = 0.00075$ and 1.

Behavior of $C(\xi, \lambda)$

$\xi \leq 0.01$

$$C' = \frac{\lambda C}{1 + \lambda} = \frac{(1 + \lambda)^2}{2\lambda}\xi$$

$\xi \geq 1$

$$C' = \frac{\lambda C}{1 + \lambda} = 1 - \frac{6\lambda}{s(1 + \lambda)^2} + \frac{8\lambda(1 + \lambda^2)}{(1 + \lambda)^4 s^3} - \frac{60\lambda(1 + \lambda^3)}{(1 + \lambda)^5 s^4}$$

$0.01 < \xi < 1$

$$C' = \frac{A_3 \xi^{B_3}}{1 + A_3 \xi^{B_3}} \tag{10}$$

A_3 and B_3 are constants determined by matching the values of C' at $\xi = 0.01$ and 1. The best fit values of matching functions A_1, B_1, A_2, B_2, A_3, and B_3 as a function of size ratio parameter, λ, are given in the Appendix.

The cross-sectional area, A_c, is an area far upstream of the target particle through which the particles flowing are capable of impacting the target particle (Fig. 2). This area can be determined by performing trajectory calculations using Eqs. 5–10. Flux of the particles through A_c gives the collision rate in a shear field as [Zeichner and Schowalter (1977)]:

$$J_{12} = -N_1 N_2 \int_{A_c} U_{12} \cdot \mathbf{n}\, dS \tag{11}$$

where N_1 and N_2 are number densities of the colliding particles, respectively; U_{12} is the relative velocity between the particles; dS is a surface element on the far upstream area; and $\mathbf{n}$ is the unit normal to the surface element dS. The far upstream cross-section is constructed by backward-integrating Eq. 5 in time with the initial conditions of $s \sim 2$ (a slight perturbation of $s = 2.01$ was included to get the collision diameter. The magnitude of this perturbation, on the order of the molecular membrane roughness of the platelet, is calculated such that the calculated hydrodynamic efficiency is insensitive to small variations in the distance between the surfaces of the colliding particles), $\phi = 0$, and different values of θ. The backward integration was carried out using the Runge-Kutta-Mercer method until the particles were so far apart (here taken to be $s = 10$) that they did not influence the flow field around each other. Performing trajectory calculations for values of θ between 0 and $\pi/2$ generates one quadrant of the upstream cross-section needed to complete the far upstream cross-section (since there is top-bottom and left-right symmetry). Numerically, the θ range was divided into 10 points and backward integrations were performed to obtain the corresponding y^* and z^* coordinates far upstream at $s = 10$. The coordinates (y^*, z^*) reside on the periphery of A_c. The flux through the far upstream area is normalized with the flux for linear trajectories (Smoluchowski limit) to yield the hydrodynamic efficiency as:

$$\epsilon_h = \frac{3}{8} \int_0^{y^*_{max}} y^* z^*\, dy^* \tag{12}$$

where $y^* = y/\bar{a}$, $z^* = z/\bar{a}$, $y^*_{max} = y_{max}/\bar{a}$, and y^*_{max} is the maximum calculated value of y^*. Numerical integration using quadrature procedures gave the hydrodynamic efficiency, ϵ_h.

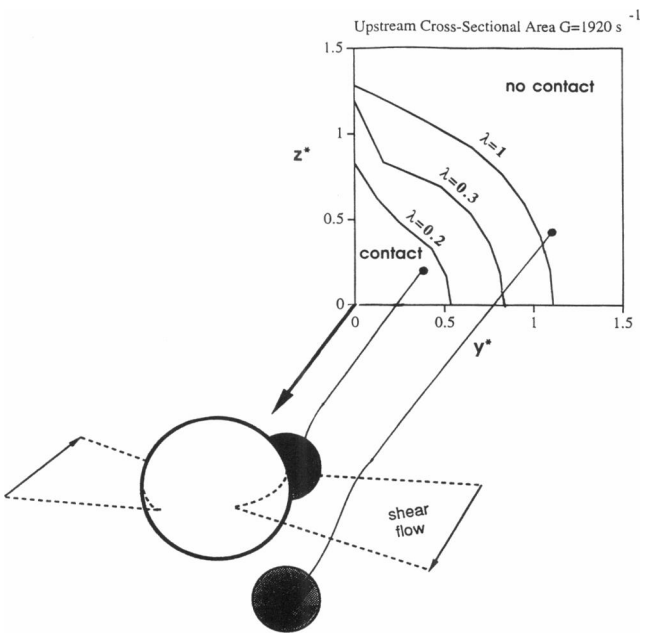

FIGURE 2 Far upstream collision cross-section of two platelet aggregates (of radii a_1 and a_2, $\lambda = a_1/a_2$) for a shear rate of $G = 1920\ s^{-1}$. Only particles flowing through these cross-sections are capable of colliding with the target particle. The particle flux through this area has been used to estimate the collision frequency. The distances y and z are made dimensionless by normalizing with the average radius ($y^* = y/\bar{a}$ and $z^* = z/\bar{a}$) where $\bar{a} = (a_1 + a_2)/2$

Collision frequency $\beta(u, v)$: receptor interactions

Platelets brought together by a shearing fluid flow are successfully bound together by fibrinogen cross-bridging to the GPIIb/IIIa receptors on the surface of the platelets [Bennett and Vilaire (1979); Marguire et al. (1980)]. Platelets are held together only if they have sufficient time to form a critical number of bonds. In reality, the collision between two activated platelets or their aggregates may display several behaviors depending on shear rate, size ratio, surface roughness, and the precise approach trajectory. At physiological shear rates, the relative low shear stresses (<30 dynes/cm^2) and short contact times (<15 ms) argue against a large viscous deformation of the platelet singlets during collision, though aggregate restructuring may occur. During collisions, rapid bond formation may cause doublet rotation. Additionally, if bond formation is insufficient to create an instantaneous doublet on contact, then complex rolling, skidding, and/or skipping movements may occur as the collision progresses. The actual collisions of platelets or their aggregates at physiologic shear rates have never been visualized in real time.

Given the multiple behaviors that are likely to occur in the real system, we utilized a hybrid concept of the "swept contact area" to model the effects of hydrodynamics on aggregate formation over the range of approach trajectories and size ratios. At the instant of contact, an initial contact area ($A_0 = \pi D_c^2/4$) is defined that depends on the particle

roughness that scales with the particle diameter. After the instant of contact the approaching particle is then allowed to flow around the target to a position of $\phi = 0$ as a growing collisional contact area A_{coll} for bond formation is swept out. The approach captures to a first-order approximation local convection effects on bond formation and the tendency of bonds to move to unstressed regions of the contact area. The overall approach is consistent with allowing bonds formed at earlier times to always contribute to aggregate stabilization by remaining in the contact area.

For two particles brought together by shear flow with collision characterized by characteristic time of collision, τ, and collision swept contact area, A_{coll}, a successful binding event takes place if

$$\left\{\int_0^{\tau} \frac{dN_b}{dt}\, dt\right\} A_{coll} \geq N_{crit} \tag{13}$$

where dN_b/dt is the net rate of formation of receptor-fibrinogen-receptor bonds per unit area and N_{crit} is the critical number of bonds needed to hold the colliding aggregates together. Following Bell (1981), the tensile force between the aggregates is assumed to be on the order of the drag force, which is assumed to be distributed equally between each of the receptors. The Stokes drag force to break bonds ($F_{drag} = 6\pi\mu R_{eff} V_{eff}$) is estimated for an effective radius of the projectile sphere in near proximity of the target as $R_{eff} = a_1(1 + \lambda)/2$. Thus, the critical number of bonds are:

$$N_{crit} = \frac{F_{drag}}{f_c} = \frac{3\pi\mu V_{eff}[a_1(1 + \lambda)]}{f_c} \tag{14}$$

where f_c is the critical force to break a bond. The effective velocity, $V_{eff}[=\sqrt{(V_r^2)+(V_\theta^2)+V_\phi^2)}]$ is the relative velocity between the particles at time of contact at s = 2.01. However, if the calculated value of N_{crit} is less than some minimum number of bonds (of order unity, taken to be equal to 2 for our calculations given the stochastic nature of bonding), then the value of N_{crit} is set equal to this minimum value. We next describe methods to estimate the time of collision, τ, and swept collision contact area, A_{coll}, for a collision characterized by size ratio parameter λ and point of contact (θ', ϕ').

The τ for a given collision initiated at θ', ϕ' on the target surface is calculated by defining a characteristic distance and velocity along the direction of approach of the particles. It is thus estimated to be:

$$\tau = \frac{a_1(1 + \lambda)\sin\theta' \sin\phi'}{v_x} \tag{15}$$

where the x component of the velocity v_x at contact is estimated as a function of V_r, V_θ, V_ϕ as:

$$v_x = \sin\theta \sin\phi V_r + \cos\theta \sin\phi V_\theta + \cos\phi V_\phi \quad \text{at } \theta', \phi' \tag{16}$$

To calculate the A_{coll} a roughness on the order of $\Delta r = 0.005a_1(1+\lambda)$ is associated with the aggregates. The magnitude of the roughness dictates the initial contact area. Lines between centers of the spheres and the edge of the contact area form a triangle with sides $a_1 + \Delta r$, $a_2 + \Delta r$, and $a_2 + a_2 + \Delta r$. The diameter of the contact area, D_c, can then be calculated, using geometric properties of a triangle, as:

$$D_c = 2(a_1 + \Delta r)\sin\theta_1 \tag{17}$$

where:

$$\theta_1 = \cos^{-1}\left[\frac{(a_1 + \Delta r)^2 + a_1(a_1 + 2a_1\lambda + 2\Delta r)}{2(a_1 + \Delta r)(a_1 + a_1\lambda + \Delta r)}\right] \tag{18}$$

The contact area diameter, D_c, then multiplied by the swept arc length gives the A_{coll} and is calculated to be:

$$A_{coll} = D_c a_1 \sqrt{(\cos\theta)^2 + (\sin\theta \sin\phi)^2}\tan^{-1}(\tan\theta \sin\phi) \quad \text{at } \theta', \phi' \tag{19}$$

The rate of formation of receptor-fibrinogen-receptor bonds per unit area, dN_b/dt, is calculated using the formalism of Bell (1979):

$$\frac{dN_b}{dt} = 2k_f\left[\frac{L(N_{rec,i} - N_b)(N_{rec,j} - N_b)}{K_d(1 + L/K_d)^2}\right] - k_r N_b \tag{20}$$

where k_f and k_r are forward and reverse rate constant for the bond formation, $N_{rec,i}$ and $N_{rec,j}$ are the number of active GPIIb/IIIa receptors per unit area on the colliding aggregates, and L is the fibrinogen concentration in the plasma. Fibrinogen binding to the GPIIb/IIIa receptors is a fast and rapidly equilibrated process [Bennett and Vilaire (1979); Calvete (1994)] of moderate affinity ($K_d = 0.1$ μM). The rate constant k_f is estimated from the diffusion limit rate of association of receptors in two dimensions as:

$$k_f = \eta \cdot [2\pi(D_i + D_j)] \quad (D_i = D_j) \tag{21}$$

where η is the effectiveness factor and D_i and D_j are the diffusion constant of receptors on the opposing membranes. Bell's original estimate of $\eta = 0.1$ (Bell, 1981) likely represents an upper limit given the orientational, steric, and membrane constraints limiting bond formation. Ideally, the value of η captures the apparent and average behavior of bond formation between real (rough) platelets, but is not a function of particle hydrodynamics. The factor "2" in Eq. 20 is a result of the fact that there is heterobinding between bound fibrinogen and free receptors on each of the colliding surfaces. Assuming that dissociation is slow for unstressed bonds [Bell (1979)] and $N_b \ll N_{rec,i}$, $N_{rec,j}$, the bond formation rate per unit area is given as:

$$\frac{dN_b}{dt} = 2k_f\left[\frac{L(N_{rec,i})(N_{rec,j})}{K_d(1 + L/K_d)^2}\right] \tag{22}$$

This approach is consistent with aggregate creation dominated by the rate of bond association without significant

TABLE 1 Values of input parameters for our model

Parameter	Value	Reference
Debye Length	0.96 Å	Van de Ven (1989)
London wavelength, λ_L	100 nM	Van de Ven (1989)
Plasma dielectric constant	78.54	
Platelet Hamaker constant, H	10^{-19} J	Hammer and Apte (1992)
Platelet zeta potential	−15 mV	Prieve and Ruckenstein (1976)
Aggregate porosity	0.4	Huang and Hellums (1993)
GP IIb/IIIa per platelet	50,000/plt	Bennett and Vilaire (1979)
[Fibrinogen]	8.8 μM	Furie and Furie (1988)
K_d for fibrinogen-GP IIb/IIIa	0.1 μM	Bennett and Vilaire (1979)
Plasma viscosity, μ	1.32 cP	
Platelet concentration	300,000/μl	Huang and Hellums (1993)
Platelet radius	1.42×10^{-4} cm	Huang and Hellums (1993)
Platelet volume	12 μm^3	Huang and Hellums (1993)
GP IIb/IIIa bond strength, f_c	5 μdynes	Bell (1981)
GP IIb/IIIa diffusion constant, D_i	10^{-10} cm^2/s	Bell (1979), Schootemeijer et al. (1993)

stress-induced bond breakage [Huang and Hellums (1993)]. Note that at 50,000 receptors/platelet and 300,000 platelet/μl in plasma containing 8.8 μM fibrinogen, only 1% of the receptors are unbound at equilibrium (K_d = 0.1 μM). At 1 μM fibrinogen, the free receptors available for binding are 10.1%. Only at a concentration of 0.1 μM are half the receptors free for binding.

Only a fraction of the particles flowing through the upstream cross-section A_c result in successful binding, depending on whether the collision time is sufficient to form enough bonds to hold colliding aggregates together. To generate the fraction of the upstream cross-sectional area through which the flowing particles will result in successful binding, we started by identifying the coordinates (s = 2.01, θ', ϕ') where the colliding particles are brought in contact. The location (y^*, z^*) inside the upstream cross-section corresponding to (θ', ϕ') were calculated by performing backward integration. Parameters τ and A_{coll} were determined using Eqs. 15 and 17 for a given collision (θ', ϕ') and then the condition given by Eq. 13 was enforced. If the condition was satisfied, the parameter $P(y^*, z^*)$ was set to unity, otherwise it was set to zero. The procedure was repeated for the entire range of collisions over θ' and ϕ' ($0 \le \theta, \phi \le \pi/2$) to generate the function $P(y^*, z^*)$, which was then used to calculate the receptor efficiency, ϵ_r, as:

$$\epsilon_r = \frac{\epsilon_{r+h}}{\epsilon_h} = \frac{3/8 \int_0^{y^*_{max}} y^* z^* P(y^*, z^*)\, dy^*}{3/8 \int_0^{y^*_{max}} y^* z^*\, dy^*} = \text{function}\left(G, \lambda, \frac{dN_b}{dt}\right) \quad (23)$$

RESULTS

Parameters for the model are given in Table 1 for calculations performed for shear rates between 50 s^{-1} and 12,000 s^{-1} corresponding to the values of C_A between 2.27×10^{-4} and 5.45×10^{-2} and C_R/C_A = 21.9 (ψ_{ref} = 1 mV). The far upstream hydrodynamic cross-section A_c for G = 1920 s^{-1} at different values of λ are shown in Fig. 2. The flux through this upstream area was used to calculate the total number of collisions (not all necessarily result in aggregation) between the aggregates. In Fig. 3, we present a surface plot of the hydrodynamic efficiency ϵ_h as a function of colliding particle size ratios (λ) and dimensionless parameter (C_A). This accounts for hydrodynamic interactions neglected by Smoluchowski in Eq. 2. For equal-sized platelet aggregates, the collision hydrodynamic efficiency increased from a value of 0.13 for G of 12,000 s^{-1} to a value of 0.29 for G of 50 s^{-1}. The corresponding values for size ratio of 0.5 were calculated to be 0.11 for G = 12000 s^{-1} and 0.26 for G of 50 s^{-1}. The collision efficiencies are much smaller for higher shear rates and small size ratios. For example, the

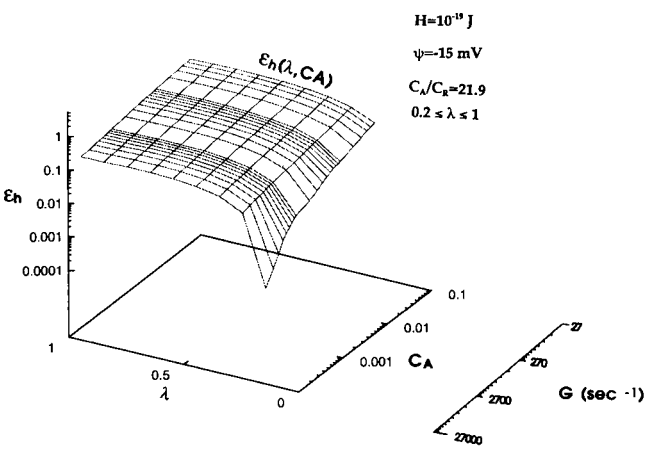

FIGURE 3 Flux of platelets or aggregates flowing through the far-upstream collision cross-section areas was used to calculate the hydrodynamic collision efficiency ϵ_h at various size ratios λ and shear rates. Hydrodynamic collision efficiency multiplied by the Smoluchowski collision frequency β_G gives the collision kernel corrected for hydrodynamic interactions between platelets of radii a_1 and a_2 ($\lambda = a_1/a_2$) at a prevailing shear rate G. Parameter C_A is a dimensionless ratio between the van der Waals and hydrodynamic forces, and is given as $2H/9\pi G\mu a_1^3$, where μ is the plasma viscosity and H is the membrane Hamaker constant. The surface plot is shown is for a constant platelet potential of −15 mV.

efficiency is only 0.04 for a size ratio of 0.3 at a shear rate of 12,000 s^{-1}. For a still smaller size ratio of 0.1, ϵ_h decreased from 0.0132 to 1×10^{-4} between shear rates of 50 and 1200 s^{-1}, suggesting that the capture of fresh singlets by an aggregated swarm is very inefficient. The hydrodynamic efficiency, ϵ_h, multiplied by the Smoluchowski collision frequency gives the total number of collisions between aggregates of size ratio λ and at shear rate G. In sheared platelet-rich plasma (PRP) (1.32 cP) with 300,000 platelet/μl, the initial collision kernel ($\epsilon_h\beta_G$) *with* hydrodynamic interactions is 375.67 $(\mu m)^3/s$ at 41.9 s^{-1} (ϵ_h = 0.295), 1928.32 $(\mu m)^3/s$ at 335 s^{-1} (ϵ_h = 0.226) and 8313.41 at 1920 s^{-1} (ϵ_h = 0.17). This corresponds to 16906, 86775 and 374103 collisions/μl per second at G = 41.9, 335, and 1920 s^{-1}, respectively. The continuum approach of this work is based on the averaging of tens of thousands of collisions each second.

For rapidly calculating the hydrodynamic efficiency, we have fitted the surface shown in Fig. 3 to the following functional form:

For $0.3 \le \lambda \le 1$

$$\epsilon_h = X_1(\lambda)(C_A)^{Y_1(\lambda)}$$

where

$$X_1(\lambda) = -0.2258\lambda^3 - 0.1579\lambda^2 + 0.7356\lambda + 0.1077$$

$$Y_1(\lambda) = -1.1866\lambda^3 + 2.7509\lambda^2 - 2.0556\lambda + 0.6411$$

For $0.2 \le \lambda < 0.3$

$$\epsilon_h = X_2(\lambda)C_A^3 + X_3(\lambda)C_A^2 + X_4(\lambda)C_A + X_5(\lambda)$$

where $X_2(\lambda) = 888.315 + 9757.45(\lambda - 0.2)$

$$X_3(\lambda) = -101.518 - 1014.68(\lambda - 0.2)$$

$$X_4(\lambda) = 4.182 + 31.32(\lambda - 0.2)$$

$$X_5(\lambda) = 0.0032 + 0.451(\lambda - 0.2)$$

For $0.1 \le \lambda < 0.2$

$$\epsilon_h = X_6(\lambda)C_A + X_7(\lambda) \quad \text{for } C_A \ge 0.005$$

where $X_6(\lambda) = 0.2217 + 7.353(\lambda - 0.1)$

$$X_7(\lambda) = 0.254(\lambda - 0.1)$$

$$\epsilon_h = 0 \quad \text{for } C_A < 0.005$$

For $\lambda < 0.1$

$$\epsilon_h = 0 \tag{24}$$

Results from the above correlation are within 4% of the values shown in Fig. 3 over the complete range of C_A and λ. This provides a useful and convenient hydrodynamic correction (with DLVO interactions) to the Smoluchowski collision kernel for colliding platelets at varying shear rates and size ratios.

Having calculated the hydrodynamics contributions of the problem, an estimate of the effectiveness factor η was needed to characterize the average and apparent rate of bond formation. Although phenomenological in nature, the effectiveness factor is commonly used to capture the overall kinetics of reactions in the presence of complex diffusion processes. The initial singlet consumption rate is the most appropriate data to estimate η for $\lambda = 1$ since the complex collision dynamics of aggregates influence the initial rate to a far lesser extent at early times. For maximally activated platelets (N_{rec} = 50,000/platelet) and half-maximally activated platelets (N_{rec} = 25,000/platelet) the overall efficiency ϵ_{r+h} was calculated for η = 0.0178 (Table 2) for G = 41.9, 335, and 1920 s^{-1}. Good agreement was obtained using η = 0.0178 with the values determined from initial platelet singlet consumption rates in flow of PRP through a tube [Bell et al. (1989)]. The model was quite sensitive to the choice of η and prevailing receptor number. Values of η that were only 0.5 or 2 times that of η = 0.0178 did not predict the experimental data in Table 2. Though the vast complexities of platelet physiology (reactivity lag times, integrin regulation, or the role of vWF) are not considered, the single parameter of η = 0.0178 provided a suitable prediction of platelet aggregation mediated by fibrinogen for shear rates between 50 and 2000 s^{-1} and modest to high degrees of ADP stimulation (Table 2). To our knowledge, this is the first estimate of η for the GPIIb/IIIa-fibrinogen cross-bridging of platelets that is based on a quantitative hydrodynamic calculation.

An additional and independent method to estimate the value of η is to apply the condition of colloidal stability for unstimulated platelets that have a low but finite number of active GPIIb/IIIa. In this approach, the head-on collision at $\theta' = \phi' = \pi/2$, which has the maximum time for bond formation, is assigned a value of η such that the criteria in Eq. 13 are just satisfied. All collisions except perfect head-on collisions achieved by secondary collision fail to provide successful aggregation. In Table 3, we report the value of effectiveness factors for which the population of unactivated platelets will be just stable for different values of receptor concentration (1000–10,000/platelet) on the unstimulated platelet surface. Again, we see that the estimated values of η for colloidal stability are in the same range as the value of η determined to predict singlet consumption in Table 2. At G = 41.9 s^{-1}, the collision times are long; however, platelets with up to ~5000 active receptors will fail to aggregate in plasma for η = 0.0178. Indeed, PRP without agonist stimulation will not aggregate at low shear despite low-level platelet activation during isolation when ≤10% of GPIIb/IIIa are active (Mazurov et al., 1996).

In Fig. 4 *A* we present the hydrodynamic far upstream cross-section for G = 41.9 s^{-1} and λ = 1. Also shown in the figure is the far upstream cross-section if particles were to follow linear trajectories (Smoluchowski limit). We also show the fraction of the area (referred to as the successful collision area) through which flowing particles will have sufficient time to form enough fibrinogen-GPIIb/IIIa bonds

TABLE 2

	0.2 μM ADP* 0–4 → 4–8 or 11 → 8–21 s	Calculated ϵ_{r+h} 25,000/platelet	1.0 μM ADP 0–4 → 4–8 s	Calculated ϵ_{r+h} 50,000/platelet
		$\bar{G}$ = 41.9 s^{-1}		
Male	0.260 → 0.0738		0.717 → 0.223	
Female	0.313 → 0.0785	0.112	0.231 → 0.131	0.206
Male	0.118 → 0.068 → 0.059			
Female	0.264 → 0.0882 → 0.108			
		$\bar{G}$ = 335 s^{-1}		
Male	0.0 → 0.0219		0.046 → 0.205	
Female	0.0259 → 0.0363	0.009	0.0247 → 0.0552	0.0496
Male	0.007 → 0.013 → 0.022			
Female	0.0174 → 0.0353 → 0.499			
		$\bar{G}$ = 1920 s^{-1}		
Male	0.00096 → 0.00319		0.005 → 0.0414	
Female	0.00037 → 0.00465	<0.001	0.009 → 0.0345	0.0086
Male	0.00198 → 0.00165			
Female	0.00062 → 0.0023			

Calculated initial collision efficiencies (ϵ_{r+h} at t = 0 and λ = 1) for an effectiveness factor of η = 0.0178 are compared with measured efficiencies for platelet aggregation at various average shear rates $\bar{G}$ in tube flow and times in PRP (300,000/μl and 37°C) with 0.2 μM or 1.0 μM ADP stimulation. In the model for 1.0 μM ADP stimulation, the maximal level of GPIIb/IIIa receptors was set at 50,000/platelet, while for 0.2 μM ADP stimulation, the receptor level was set half-maximally to 25,000/platelet.
*Data from Table 2 and 3 of Bell, 1989.

to hold the colliding particles together. In Fig. 4 *A*, ϵ_{r+h} = 0.206 for η = 0.0178 and N_{rec} = 50,000/platelet. For the same value of η and N_{rec}, the corresponding upstream area for G = 335 s^{-1} and λ = 1 are shown in Fig. 4 *B* and the overall efficiency (ϵ_{r+h}) is calculated to be 0.0496, in good agreement with values estimated by Bell et al. (1989) for this condition.

The prediction of hydrodynamic and overall efficiency as a function of colliding particles size ratio parameter, λ, for these shear rates of 41.9 and 335 s^{-1}, is shown in Fig. 5 *A* for maximally activated platelets (N_{rec} = 50,000/platelet). The collision and aggregate formation frequency is much more efficient for equal-sized particles than for unequal-sized particles. The corresponding ϵ_{r+h} predictions for only half the receptor concentration on the platelet surface are presented in Fig. 5 *B* for 41.9 and 335 s^{-1} (ϵ_h is the same as in Fig. 5 *A*). As expected, ϵ_{r+h} is highly sensitive to the number of active receptors. In the model, the calculation of ϵ_{r+h} depended on the bond formation rate and thus to the value chosen for the effectiveness factor, η. In Fig. 5 *C*, we show the predicted dependence of ϵ_{r+h} for different values of η for maximally activated platelets (50,000 receptors/platelet) in sheared PRP. However, for a single value of η = 0.0178, we were able to predict ϵ_{r+h} over a large range of shear rates in agreement with the efficiencies determined from platelet aggregation experiments in tube flow (Table 2).

TABLE 3

N_{rec}/platelet	η_{max} G = 41.9 s^{-1}	η_{max} G = 335 s^{-1}
1000	0.623	>1
2000	0.178	>1
3000	0.0712	1
4000	0.0445	0.267
5000	0.0267	0.089
6000	0.0178	0.0712
7000	0.0178	0.0534
8000	0.0089	0.0356
9000	0.008	0.0178
10,000	0.00623	0.0089

Value of effectiveness factor, η, at which platelet populations are just stable for different number of active GP IIb/IIIa receptors on the platelet surface. For η = 0.0178, platelets with up to 5000 active receptors will not aggregate at G = 41.9 s^{-1} and the suspensions are stable.
Values above the rule are stable, values below are unstable.

In calculating these efficiencies, primary collisions dominate the total number of collisions. Secondary collisions (orbitlike trajectories, Fig. 6) constitute only a small fraction of the total number of collisions. However, at high shear rates (>750 s^{-1}), these become important as these are the only collisions that are calculated to provide enough time to result in successful aggregate formation via fibrinogen. For these shear rates, the primary encounters result in glancing collisions far away from the stagnation point, producing an insufficient number of bonds during collision to hold the colliding aggregates together. The secondary upstream area forms a thin region just outside the primary hydrodynamic upstream area (based on which ϵ_h was calculated) in the mirror image quadrant. At higher shear rates, particle flux through the secondary region was used for calculating the efficiency over the range of λ. For G = 1920 s^{-1} and λ = 1, ϵ_{r+h} is calculated to be 0.0086, a value in agreement with measurements of Bell et al. (1989). Though less frequent, secondary collisions may extend the shear rates range at which fibrinogen can mediate successful aggregation. We predict that secondary collisions occur and can result in

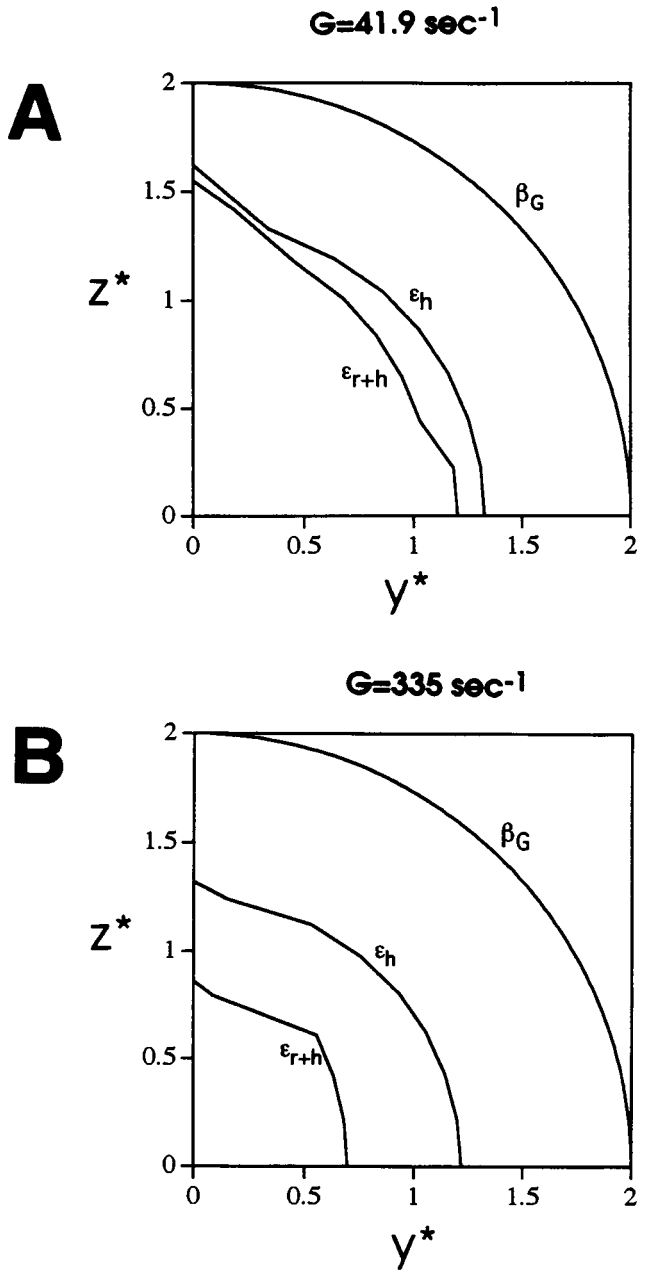

FIGURE 4 Smoluchowski, hydrodynamic, and successful (hydrodynamic + receptor) far-upstream cross-section area for $\lambda = 1$ and shear rates of $G = 41.9\ s^{-1}$ (*A*) and $335\ s^{-1}$ (*B*). The Smoluchowski upstream area is calculated considering platelets follow linear trajectories, while the hydrodynamic collision area is determined from detailed hydrodynamics interactions between colliding aggregates. Whereas the particle flux through the hydrodynamic cross-section represents the collision rate between aggregates of radii a_1 and a_2, the fraction of these collisions that is successful is represented by the particle flux through the overall (hydrodynamic + receptor) upstream cross-section area. For calculating the cross-section area for successful aggregation, the effectiveness factor of fibrinogen-GPIIb/IIIa interaction was taken to be $\eta = 0.0178$.

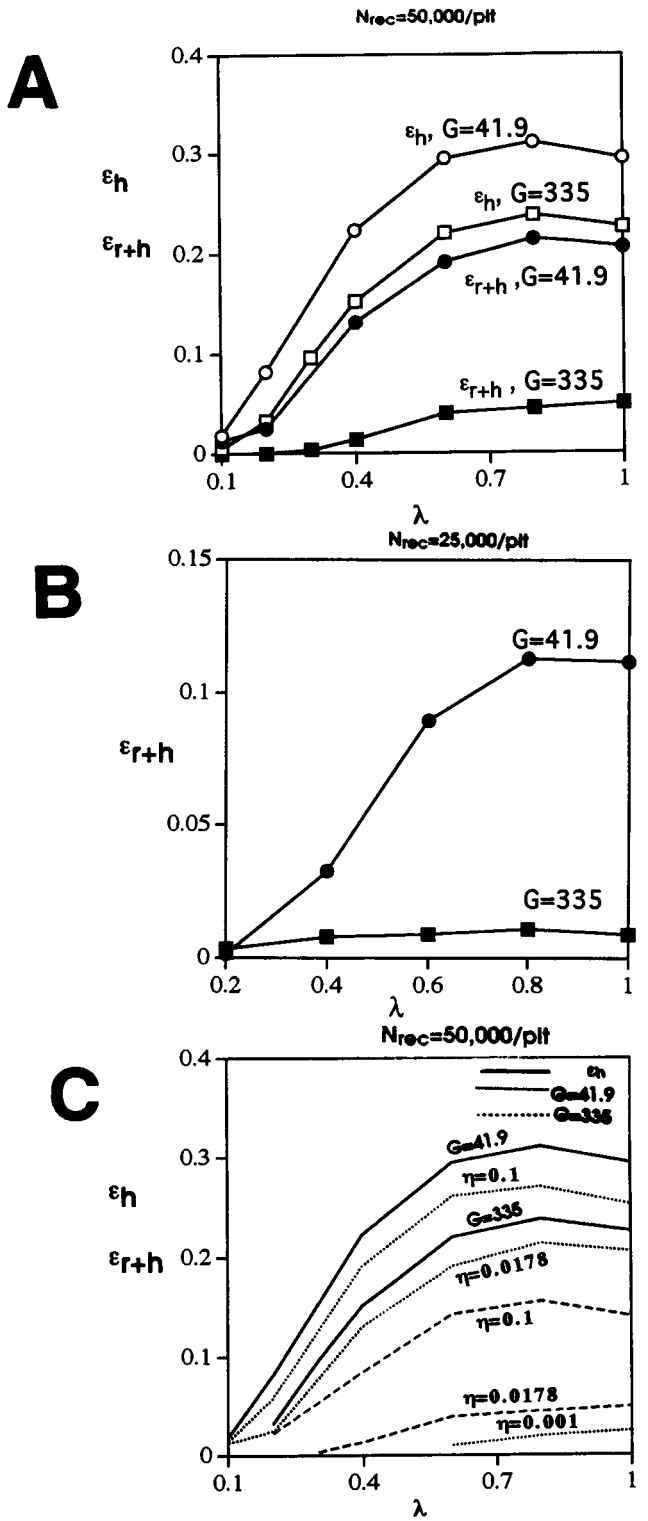

FIGURE 5 Sensitivity of hydrodynamic collision efficiency (ϵ_h) and successful collision efficiency (ϵ_{r+h}) to the particle size ratio, λ, is shown for shear rates 41.9 and $335\ s^{-1}$ and at 50,000 GPIIb/IIIa receptors per platelet (*A*) or 25,000 GPIIb/IIIa receptors per platelet (*B*). The value of effectiveness factor for the GPIIb/IIIa-fibrinogen interaction was taken as $\eta = 0.0178$. The sensitivity of ϵ_h and ϵ_{r+h} to the effectiveness factor is also shown in (*C*).

aggregation. To date, neither direct nor secondary collisions have been visualized at higher shear rates.

The collision kernel $\epsilon_{r+h}\beta_G$ as a function of G, λ, and dN_b/dt were employed in a population balance framework to

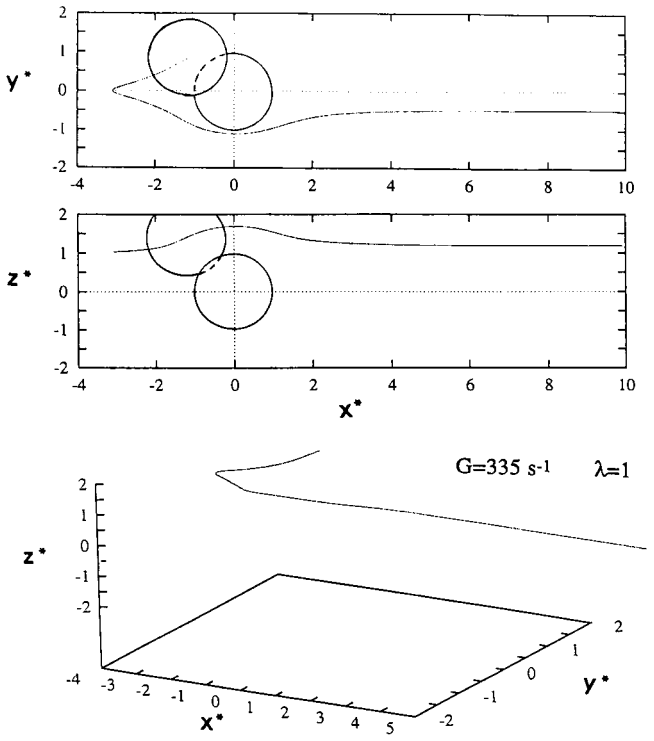

FIGURE 6 For large shear rates ($G > 750\ s^{-1}$), secondary collisions (orbitlike trajectories) are the only collisions which can provide enough contact time during collision to form sufficient bonds to hold the colliding aggregates together. For these shear rates, the primary encounters result in collision far away from the stagnation point, resulting in formation of an insufficient number of bonds during collision to hold the colliding aggregates together. A typical secondary trajectory is shown for a platelet of radius $a_1 = 1.5\ \mu m$ colliding with another platelet of the same radius in a shear field at a shear rate $G = 335\ s^{-1}$ (point of contact $\theta' = \pi/4$, $\phi' = -3\pi/10$)

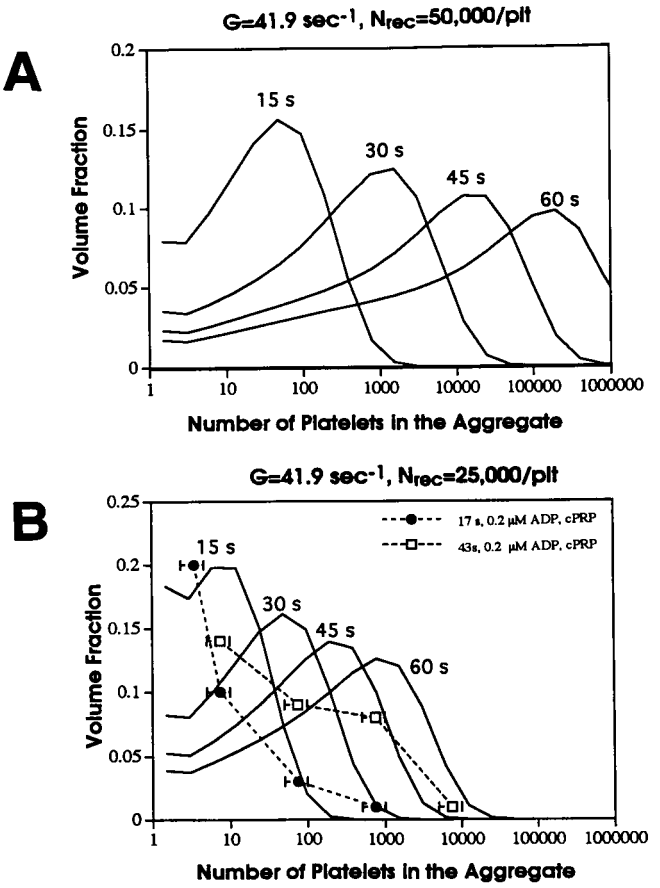

FIGURE 7 The overall collision efficiency calculated using two-body collision theory taking into account hydrodynamic effects and receptor interaction was used in a population balance to predict the evolution of size distributions of population of platelets aggregation in a shear flow. Size distributions at various times are shown for a shear rate of $41.9\ s^{-1}$ and 50,000 GPIIb/IIIa receptors per platelet (*A*) and 25,000 GPIIb/IIIa receptors per platelet (*B*). The initial distribution ($t = 0$) is considered to be monodispersed, comprised of 300,000 singlet platelets per μl. For platelets of volume ($12\ \mu m^3$) and aggregates that have a porosity of 0.4, N particles $\times$ 20 = aggregate volume (μm^3). Data is shown from Bell et al. (1989 a,b).

predict the evolution of size distribution of populations of platelets undergoing aggregation in a shear field. In Figs. 7 and 8, we show the predicted size distributions at different times for $G = 41.9\ s^{-1}$, $335\ s^{-1}$, and $1920\ s^{-1}$, starting with a monodispersed population comprising 300,000 platelets/μl. Also shown in these figures is the observed distributions by Bell et al. (1989a,b; 1990) for platelet aggregation in citrated PRP flowing through a tube at a corresponding average $\bar{G}$. Our predictions based on a single factor (η) obtained from singlet consumption data are in reasonable, though not complete, agreement with the observations. While maximal activation of receptors (50,000/platelet) is expected at high dosage of ADP ($\geq 1\ \mu M$), for our calculations we assumed that only half the receptors are expressed at low dosage of ADP ($0.2\ \mu M$). For shear rate of $G = 41.9\ s^{-1}$ and 50,000 receptors per platelet, we predict in Fig. 7 *A* very rapid aggregation and formation of extremely large aggregates, since ample time is available for bond formation during collision. Bell et al. (1989b) noted similar aggregate formation at 1 μM ADP at $41.9\ s^{-1}$, as was seen at $335\ s^{-1}$ (with a peak around 5000 platelets per aggregate at 43 s, as in Fig. 8 *A*). However, at low shear rates of $G = 41.9\ s^{-1}$ and high dosage of 1 μM ADP stimulation at which near maximal activation of receptors is expected, aggregates containing $>\sim$10,000 singlets cannot be detected with an aperture diameter of 100 μm used in a Coulter counter setup. For $G = 41.9\ s^{-1}$, the calculated distributions for 25,000 receptors/platelet were in good agreement with observed distributions for 0.2 μM ADP stimulation (Fig. 7 *B*). However, a large singlet peak that coexists with large aggregates seen in the experimental data was not predicted by our model. This singlet peak likely represents the inert fraction of platelets in the populations at modest levels of ADP stimulation. Indeed, Goldsmith et al. (1994) report only 76% of the platelets were activated at 0.2 μM ADP and $\sim$89% were activated at 100 μM ADP under nonflow conditions. For $G = 335\ s^{-1}$ and 50,000 receptors/platelet, the agreement with experiments was again seen to be quite reasonable (Fig. 8 *A*). For higher shear rates ($G = 1920\ s^{-1}$) the model underpredicted the aggregation rates

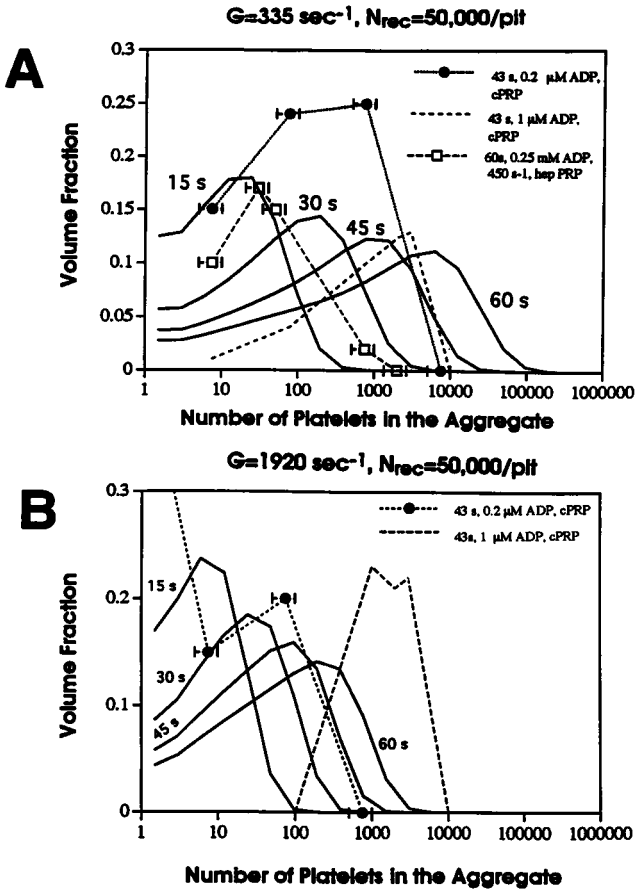

FIGURE 8 The overall collision efficiency calculated using two-body collision theory taking into account hydrodynamic effects and receptor interactions was used in a population balance to predict the evolution of size distributions of population of platelets aggregation in a shear flow. Size distributions at various times are shown for 50,000 GPIIb/IIIa receptors per platelet and shear rate of 335 s^{-1} (*A*) and 1920 s^{-1} (*B*). The initial distribution (t = 0) is considered to be monodispersed, comprised of 300,000 singlet platelets per μl. Data is shown from Bell et al. (1989a,b) for citrated PRP (cPRP) and from Huang and Hellums (1993b) for heparinized PRP (hep PRP). To obtain the height of the peak for the observed distributions with 1 μM ADP stimulation, the size spectrum was again divided into bins in a geometric series such that the smallest size in the ith bin has 2^i monomers and largest size has 2^{i+1} monomers. The volume fraction in each bin as a fraction of the peak volume fraction was calculated from the observed distribution and then the peak height was calculated by imposing the condition that the sum of the volume fractions in all the bins equal unity.

and sizes (Fig. 8 *B*). To obtain the peak height for observed distributions with 1 μM ADP stimulation in Fig. 8, *A* and *B*, the peak height was calculated by imposing the condition that the sum of the volume fractions in all the bins equals unity. The agreement of the predicted distributions for G = 1920 s^{-1} and 50,000 receptors/platelet with observed data for 0.2 μM stimulation rather than 1 μM ADP stimulation was somewhat contrary to expectation, since this level of receptor concentration is more likely achieved at higher dosage of ADP (1 μM). For 1920 s^{-1} and 25,000 receptors/platelet, the predicted successful collision efficiency ($\epsilon_{r+h} < 0.001$) was so small that it could not be resolved numerically by our methods. Even at 50,000 receptors, we underpredict aggregation at 1 μM ADP stimulation of cPRP (Fig. 8 *B*) at G = 1920 s^{-1}. The underprediction in the aggregation rates is likely explained by the fact that vWF is especially important in mediating aggregation at high shear rates, but is not considered in the model. Also, the flow through the porous aggregates, platelet protopods, and aggregate roughness are not included in the model—factors that are expected to increase the hydrodynamic and successful collision efficiency. Also, the size distribution data of Bell et al. (1989 a,b; 1990) is for platelet aggregation for flow in a tube, where a range of shear rates exist from the tube wall inward where $\bar{G}$ represents an average of the total range. Slower aggregation rates were observed by Huang and Hellums (1993) for platelet aggregation in heparinized PRP in a cone and plate viscometer setup (Fig. 8 *A*) at a slightly higher shear rate of 450 s^{-1}. Although some disaggregation is expected for low ADP and G = 450 s^{-1}, the differences in the experiments shown in Fig. 8 *A* are interesting since no lag time would be expected in heparinized PRP, while a lag time is expected for citrated PRP.

In Fig. 9 we present the predicted platelet singlet consumption rate for G = 41.9 s^{-1} and 335 s^{-1} for 50,000 and 25,000 GPIIb/IIIa receptors per platelets. Also shown in the figure is the observed singlet consumption rates for whole blood (WB) and citrated PRP in tube flow [Goldsmith et al. (1994)]. Our results for 50,000 GPIIb/IIIa receptors/platelet (Fig. 9 *A*) were in good agreement with rates observed in whole blood, where a high degree of activation of the receptors is expected even at 0.2 μM ADP due to release of ADP by red blood cells. In either simulations or experiments with WB, platelets aggregate more rapidly at G = 41.9 s^{-1} than at G = 335 s^{-1}, possibly due to longer collision times for bond formation. For shear rate of 335 s^{-1} and 25,000 receptors/platelet, the predicted singlet consumption rates in Fig. 9 *B* were significantly faster than those observed at G = 41.9 or 335 s^{-1} with low ADP stimulation (0.2 μM). For calculation purposes, the model considers all the platelets to behave uniformly. At low shear rates and low levels of ADP stimulation, a significant fraction of the platelets are likely to be inert [Goldsmith et al. (1994)], thereby slowing the aggregation kinetics once reactive singlets are consumed. The relatively high efficiency of the initial platelet collisions at G = 41.9 s^{-1} (see Table 2) is in contrast to the relatively slow platelet consumption at longer times, as seen in Fig. 9 *B*. Changes in receptor function during the course of aggregation (due to internalization, etc.) might result in attenuation in the singlet consumption rate at later times for G = 41.9 s^{-1}. Predictions for G = 335 s^{-1} and 25,000 receptors/platelet (0.2 μM ADP stimulation) were within 15% of the observed rates for female donors.

DISCUSSION

We have calculated the intermediate range behavior of two unequal-sized particles in a linear shear field using the

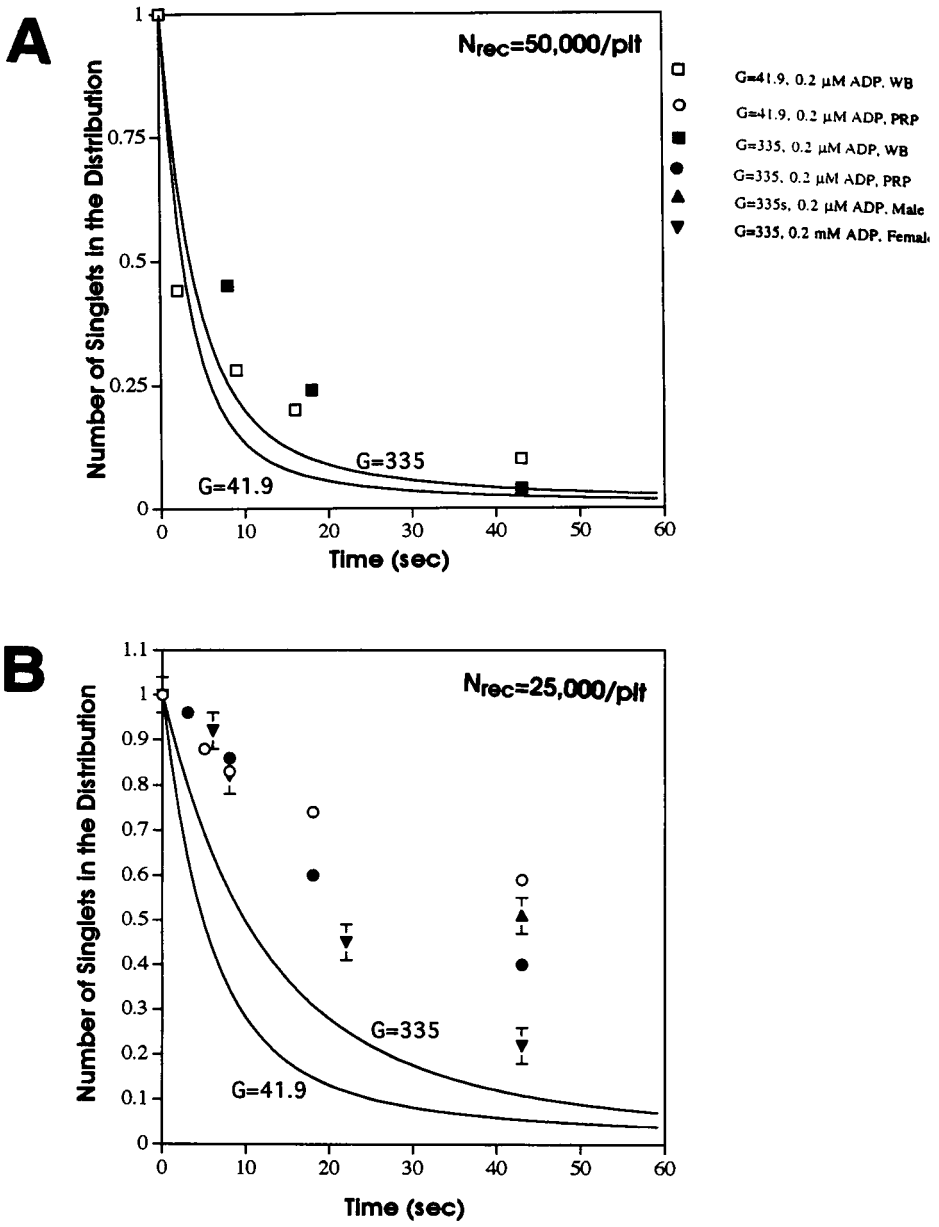

FIGURE 9 The singlet consumption rate in a population of platelets undergoing aggregation in shearing plasma flow. The initial distribution ($t = 0$) is considered to be monodispersed, comprised of 300,000 singlet platelets per μl. The singlet consumption rate has been shown for shear rates of $G = 41.9$ and 335 s^{-1} and for 50,000 GPIIb/IIIa receptors per platelet (*A*) and 25,000 GPIIb/IIIa receptors per platelet (*B*). Data is shown from Goldsmith et al. (1995).

asymptotic limits of very small separation and very large separation to generate the entire flow field around the two colliding spheres. Results from our procedures were found to be within 2% of the results in the literature that used detailed hydrodynamic calculations in the intermediate regime over a range of size ratios.

For an effectiveness factor of $\eta = 0.0178$ and apparent $k_f = 1.78 \times 10^{-11}$ cm^2/s, the initial singlet collision efficiency is predicted over a range of shear rates from 50 to 2000 s^{-1} (Table 2). The apparent rate of bond formation between fully activated platelets (50,000 receptors/platelet) in the presence of plasma levels of fibrinogen (8.8 μM) is on the order of 0.1925 bonds/μm^2 per ms. In plasma, only ~500 GPIIb/IIIa receptors on each platelet are free for complexation with the fibrinogen-GPIIb/IIIa receptors (49,500/platelet) on the opposing platelet. Also, this value of $\eta = 0.0178$ is consistent with the stability criteria for unactivated platelets in low shear, where bond formation is very favorable due to large contact times. This model predicts several aspects of platelet aggregation (excluding the effects of inert singlets in the experimental data) such as: 1) singlet consumption rates and particle size distribution evolution at varying shear rates and platelet activation can be characterized by a single reaction parameter, η; 2) secondary collisions can provide sufficient time for fibrinogen mediated aggregation at high G; 3) fibrinogen is very inefficient at $G = 1920$ s^{-1} in aggregating platelets; and 4) free GPIIb/IIIa in equilibrium with high fibrinogen (8.8 μM) is sufficient to mediate aggregation for $G < 2000$ s^{-1} if η is on the order of 10^{-2}.

Savage et al. (1996) have recently studied the mechanisms of platelet adhesion to various thrombogenic sur-

faces. Platelet adhesion to the surface has been shown to be mediated through fibrinogen and vWF. Fibrinogen supports the platelet surface by binding to the GPIIb/IIIa receptors, while vWF binding is through $GPIb_{\alpha}$ and $\alpha_{IIb}\beta_3$. Platelet deposition mechanisms to immobilized fibrinogen and vWF under flow are different in nature. The fibrinogen attachment was seen to be irreversible and was less efficient with increasing shear rates. On the other hand, vWF-mediated attachments were efficient for large shear rates, but became irreversible only gradually. Consistent with this finding, our calculations indicate that for the reactivity manifest at $G = 41.9\ s^{-1}$ where $\eta = 0.0178$, fibrinogen becomes very inefficient to mediate aggregation at high G and vWF is likely necessary to extend collision contact times at high G to allow successful aggregation in bulk shear flow.

The values of platelet Hamaker constant and electrostatic potential are not known very accurately, but they are not likely to be critical in predicting the platelet population evolution. Results with $\psi = -60$ mV, where the platelet membrane potential was used instead of the zeta potential, gave similar results. More than two body collisions have been neglected in our calculations. This assumption is suitable for PRP where platelets are <1% by volume and may not be too limiting in whole blood, since the work of Goldsmith et al. (1995) has shown that only a modest prolongation of collision times at low shear rate is observed in the presence of high-hematocrit RBC ghosts.

The model is idealized in the sense that the initial platelet population is taken as completely uniform in size, shape (spherical), and active GPIIb/IIIa surface density. In reality, activated platelets have protopods and platelet aggregates are rough and porous—two effects not considered in the collision hydrodynamics. In vitro experiments typically begin with a size distribution of platelets, some of which are activated (as indicated by P-selectin or active GPIIb/IIIa) even for very careful isolation conditions. Also, receptor function changes over the course of the aggregation due to phosphorylation, internalization, etc. Multiple receptors and ligand epitopes are potentially involved in platelet aggregation in sheared suspensions (GPIb, vWF, fibrinogen, RGD domains, etc.). A significant number of platelets are unresponsive to low-level agonist stimulation, and these inert singlets undergo collisions that are unsuccessful. This inert population results in bimodal population distribution at later times where a significant singlet peak coexists with large multimers. This is not expected theoretically for a uniform population of equally reactive particles. Experimental data are often obtained in tube flow in order to recreate the vascular condition; however, a range of shear rates are manifest from the tube wall inward when compared to cone and plate viscometer systems that create a single shear rate.

While we recognize that platelets and their aggregates are rough and nonspherical with pseudopods, hydrodynamics and collisions of such morphologically complex aggregates are not yet completely understood. In light of this, assuming platelets and their aggregates are smooth spheres is a reasonable first approximation. The boundary element method (BEM) and continuum methods have been recently used [Pakdel and Kim (1991); DaCunha and Hinch (1996); Davis (1992)] to study some aspects of interaction between particles with microscale roughness; however, these approaches are not yet suitable for complete characterization of collision between rough aggregates in shear flow. An interesting approximate pseudocontinuum representation of these aggregates was put forward by Frojmovic et al. (1990) who assumed that rough platelet aggregates with pseudopods can be viewed as a composite sphere comprised of a spherical core of radius a surrounded by a porous shell with outer radius b. Even though this composite sphere representation of platelets with spikes (3–4 in number) may have limitations, we have calculated the hydrodynamic radius of the composite sphere using the formulation of Masliyah et al. (1987). For $a = 1.42\ \mu$m, roughness on the order of 100 nm and permeability of $6.3\ \mu m^2$ [Frojmovic et al. (1990)], the hydrodynamic radius of such a composite sphere was calculated to be only 0.5% more than the radius of the inner core, suggesting our representation of platelets as smooth spheres to be a reasonable one. The mobility functions in shear flow [$A(\xi)$ and $B(\xi)$] to characterize collisions between porous particles are not known and are the subject of ongoing investigation beyond the scope of the present work. An approximate method to predict collision frequency between morphologically complex particles has been suggested by Li and Logan (1997); Kusters et al. (1997); and Torres et al. (1991) involving conducting trajectory calculations considering the composite sphere to behave as a smooth solid sphere with a radius equal to the hydrodynamic radius of the composite sphere, and the outer radius b representing the distance within which another aggregate must approach for collision to take place. DaCunha and Hinch (1996) also reached the same conclusion, that a rough sphere hydrodynamically behaves similarly to a smooth sphere and roughness only influences the distance within which particles are to be brought together for a collision to take place. This approach will be explored in the future to study the sensitivity to morphology on the collision dynamics of the platelets.

Frojmovic et al. (1990) report that platelets can be viewed as oblate spheroids with aspect ratio ¼. For length = 3.6 μm and width = 0.9 μm the hydrodynamic radius is calculated to be 1.47 μm [pg 148, Happel and Brenner (1983)] compared to 1.2 μm calculated based on the volume of an equivalent sphere. The hydrodynamic efficiencies based on the hydrodynamic and volume equivalent radius were seen to be within 8.7% for shear rates between 50 s^{-1} and 2000 s^{-1}, again suggesting the approximation of considering platelets as quasispherical to be a reasonable one.

There is no reason to expect the full range of experimental observations to be predicted with a model based on two-body collision for DLVO interactions of spheres uniformly covered with GPIIb/IIIa receptors in the presence of fibrinogen. Still, key elements of platelet aggregation are captured in the model by assuming that aggregate formation is dominated by the forward rate of bond formation and by

assuming that the aggregates are spherical and have an average receptor density consistent with the singlet density. The model provides hydrodynamic correction factors for collision of platelets and their aggregates at any given shear rate. The model provides predictions testable by population data in which the effect of the shear rate (collision rate), shear stress (force on bonds), and number of bonding pairs can be deconvoluted by varying the shear rate, viscosity, agonists, and fibrinogen levels.

For better understanding of multicellular aggregation mediated through multiple receptors [Taylor et al. (1996)], tools need to be developed to analyze heteroaggregation behavior. These tools can then be applied to study the aggregation of platelets when some of the platelets are inert (or there is a distribution of receptors on platelet surfaces) and simultaneous platelet-platelet and platelet-neutrophil aggregation occurs in coagulating plasma. With an understanding of bulk aggregation, it may be possible to eventually predict platelet and neutrophil deposition rates and thrombus growth at a damaged vessel wall.

APPENDIX

Behavior of functions *A*, *B*, *C*

The correlations for functions $A(\xi, \lambda)$, $B(\xi, \lambda)$, and $C(\xi, \lambda)$ as given in Eqs. 12–14 have been used in performing trajectory calculations. The comparison of behavior of these functions with results in the literature using detailed hydrodynamic calculations in the intermediate regime over a range of size ratios have been done, and the case for $\lambda = 0.5$ is shown in Fig. A1. As can be seen, the agreement between the two is very good and they are within 2% of each other. Identical agreement was also seen at $\lambda = 0.1, 0.2$, and 1 (not shown). The constants in Eqs. 12–14 were calculated and fitted to following functional forms:

$$A_1(\lambda) = \exp[2.217\lambda^3 - 6.301\lambda^2 + 6.2595\lambda - 0.653]$$

$$B_1(\lambda) = -6.438\lambda^5 + 19.133\lambda^4 - 21.724\lambda^3 + 11.539\lambda^2 - 2.508\lambda + 1.011$$

$$A_2(\lambda) = 2.805\lambda^3 - 5.3421\lambda^2 + 3.353\lambda - 1.147$$

$$B_2(\lambda) = -3.072\lambda^3 + 5.92\lambda^2 - 3.767\lambda + 1.2687$$

$$A_3(\lambda) = 37.79\lambda^4 - 100.016\lambda^3 + 95.906\lambda^2 - 39.98\lambda + 7.30 \quad \text{for } 0.1 \le \lambda \le 1$$

$$= 13.74 - 135.85(\lambda - 0.03) \quad \text{for } 0.03 \le \lambda < 0.1$$

$$B_3(\lambda) = -0.0864\lambda^3 + 0.268\lambda^2 - 0.279\lambda + 0.9344 \quad \text{for } 0.1 \le \lambda \le 1$$

$$= 0.903 + 0.086(\lambda - 0.03) \quad \text{for } 0.03 \le \lambda < 0.1 \quad \text{(A1)}$$

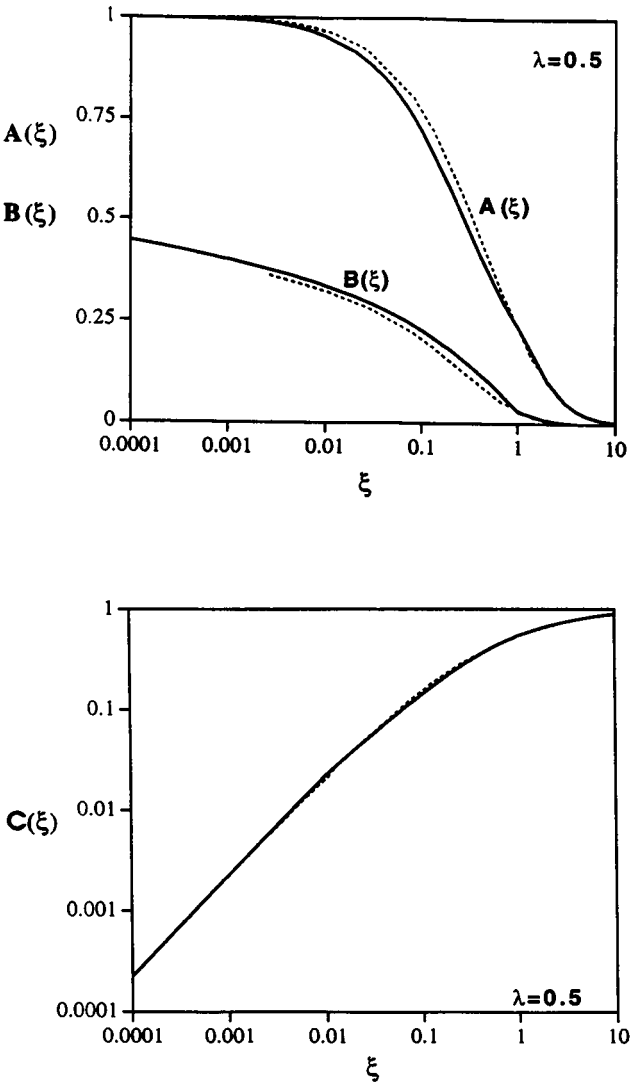

FIGURE A1 Behavior of mobility functions $A(\xi)$, $B(\xi)$, and $C(\xi)$ with dimensionless separation distance, ξ, between the colliding particles were needed to integrate Eq. 9 to perform the trajectory calculations. We have calculated the intermediate hydrodynamic behavior of two unequal-sized particles in a shear field by using the behavior in the asymptotic limits of small separation and very large separations. Also shown in the figures (*dotted line*) are behavior of these functions using detailed hydrodynamic solution as reported by Adler (1981a) and Batchelor and Green (1972). Although here we only show the comparison for $\lambda = 0.5$, agreement within 2% was also seen for other values of λ of 0.1, 0.2, and 1 (not shown).

Solution of the population balance equation

The two-body theory developed above to predict the collision frequency $\epsilon_{r+h}\beta_G$ was used in a population balance framework to calculate the evolution of size distributions of platelets undergoing aggregation in a shear field. A large number of equations need to be simultaneously integrated as a result of PBE of the form shown in Eq. 1. To circumvent this problem, we use the sectional method suggested by Hounslow et al. (1988). In this scheme, the size spectrum is divided into M sections in a geometric series such that the smallest size in the ith section has 2^i monomers and the largest size has 2^{i+1} monomers. The bookkeeping of particle number densities is performed in each of the sections and the rate of change of

number density in the ith section is given as:

$$\frac{dN_i}{dt} = N_{i-1}\sum_{j=1}^{i-2} 2^{j-i+1}\beta_{i-1,j}N_j + \tfrac{1}{2}\beta_{i-1,i-1}N_{i-1}^2 - N_i\sum_{j=1}^{i-1} 2^{j-i}\beta_{i,j}N_j - N_i\sum_{j=i}^{M}\beta_{i,j}N_j \quad \text{(A2)}$$

where N_i is the number density of particles in the ith section and $\beta_{i,j}$ is the collision frequency of spherical particles in the ith and jth intervals. Collision frequency $\beta_{i,j}$ is estimated using Eqs. 6 and 27, and these are calculated for arithmetic mean volume in each section. For a given set of shear rate and receptor concentration, the number of bins (value of M) chosen for integration are such that the total mass of the system is conserved. Eq. A1 is integrated numerically by Runge-Kutta-Mercer to predict the evolution of platelet size distributions. With the population distribution N_i, it is straightforward to calculate the ensemble-averaged light scattering properties as

$$LS_{a0} = k\left(\sum_{i=1}^{M} N_i v_i^2\right) \quad \text{(Chang and Robertson (1976))}$$

where k is a constant. The light transmission typical of aggregometry is less sensitive to the formation of aggregates as large as 10 platelets [Goldsmith et al. (1994)].

The authors would like to thank Dr. Johannes Nitsche for helpful discussions.

This work was supported by National Institutes of Health Grant HL 56621 and National American Heart Association Grant 96-6670. S.L.D. is a recipient of the NSF National Young Investigator award and P.T. is a recipient of a postdoctoral fellowship from the American Heart Association, Southeastern Pennsylvania Affiliate.

REFERENCES

Adler, P. M. 1981a. Heterocoagulation in shear flow. *J. Colloid Int. Sci.* 83:106–115.

Adler, P. M. 1981b. Interaction of unequal spheres: I. Hydrodynamic interactions: colloidal forces. *J. Colloid Int. Sci.* 84:461–473.

Batchelor, G. K., and J. T. Green. 1972. The hydrodynamic interaction of two small freely moving spheres in a linear flow field. *J. Fluid Mech.* 56:375–400.

Bell, G. I. 1979. A theoretical model for adhesion between cells mediated by multivalent ligands. *Cell Biophys.* 1:133–147.

Bell, G. I. 1981. Estimate of the sticking probability for cells in uniform shear flow with adhesion caused by specific bonds. *Cell Biophys.* 3: 289–304.

Bell, D. N., S. Spain, and H. L. Goldsmith. 1989a. Adenosine diphosphate-induced aggregation of human platelets in flow through tubes. I. Measurement of concentration and size of single platelets and aggregates. *Biophys. J.* 56:817–828.

Bell, D. N., S. Spain, and H. L. Goldsmith. 1989b. Adenosine diphosphate-induced aggregation of human platelets in flow through tubes. II. Effect of shear rate, donor sex, and ADP concentration. *Biophys. J.* 56: 829–843.

Bell, D. N., S. Spain, and H. L. Goldsmith. 1990. The effect of red blood cells in the ADP-induced aggregation of human platelets in flow through tubes. *Thromb. Haemostasis.* 63:112–121.

Belval, T. K., and J. D. Hellums. 1986. Analysis of shear induced platelet aggregation with population balance mathematics. *Biophys. J.* 50: 479–487.

Bennett, J. S., and G. Vilaire. 1979. Exposure of platelet fibrinogen receptors by ADP and epinephrine. *J. Clin. Invest.* 64:1393–1401.

Calvete, J. J. 1994. Clues for understanding the structure and function of a prototypic human integrin: the platelet glycoprotein IIb/IIIa complex. *Thromb. Haemostasis.* 72:1–15.

Chang, H. N., and C. R. Robertson. 1976. Platelet aggregation by laminar shear and Brownian motion. *Ann. Biomed. Eng.* 4:151–183.

DaCunha, F. R., and E. J. Hinch. 1996. Shear induced dispersion in a dilute suspension of rough spheres. *J. Fluid Mech.* 309:211–223.

Davis, R. H. 1992. Effects of surface roughness on a sphere sedimenting through a dilute suspension of neutrally buoyant spheres. *Phys. Fluids A.* 4:2607–2619.

Frojmovic, M., K. Longmire, and T. G. M. Van de Ven. 1990. Long-range interactions in mammalian platelet aggregation II. The role of platelet pseudopod number and length. *Biophys. J.* 58:309–318.

Frojmovic, M. M., T. E. O'Toole, E. F. Plow, J. C. Loftus, and M. H. Ginsberg. 1991. Platelet glycoprotein IIb-IIIa confers fibrinogen and activation dependent aggregation on heterologous cells. *Blood.* 78: 369–376.

Furie, B., and B. C. Furie. 1988. The molecular basis of blood coagulation. *Cell.* 53:505–518.

Goldsmith, H. L., D. N. Bell, S. Braovac, A. Steinberg, and F. McIntosh. 1995. Physical and chemical effects of red cells in the shear-induced aggregation of human platelets. *Biophys. J.* 69:1584–1595.

Goldsmith, H. L., M. Frojmovic, S. Braovac, F. McIntosh, and T. Wong. 1994. Adenosine diphosphate-induced aggregation of human platelets in flow through tubes. III. Shear and extrinsic fibrinogen dependent effects. *Thromb. Haemostasis.* 71:78–90.

Hammer, D. A., and H. Apte. 1992. Simulation of cell rolling and adhesion. *Biophys. J.* 63:36–57.

Happel, J., and H. Brenner. 1983. Low Reynolds-Number Hydrodynamics. Nijhoff, Boston.

Hounslow, M. J., R. L. Ryall, and V. R. Marshall. 1988. A discritized population balance for nucleation, growth and aggregation. *AIChE J.* 34:1821–1834.

Huang, P. Y., and J. D. Hellums. 1993a. Aggregation and disaggregation kinetics of human blood platelets. I. Development and validation of a population balance method. *Biophys. J.* 65:334–343.

Huang, P. Y., and J. D. Hellums. 1993b. Aggregation and disaggregation kinetics of human blood platelets. II. Shear-induced platelet aggregation. *Biophys. J.* 65:344–353.

Huang, P. Y., and J. D. Hellums. 1993c. Aggregation and disaggregation kinetics of human blood platelets. III. Disaggregation under shear stress of platelet aggregation. *Biophys. J.* 65:354–361.

Kim, S., and S. J. Karrila. 1991. Microhydrodynamics. Buttersworth, Boston.

Kusters, K. A., J. G. Wijers, and D. Thoenes. 1997. Aggregation kinetics of small particles in agitated vessels. *Chem. Eng. Sci.* 52:107–121.

Li, X., and B. E. Logan. 1997. Collision frequencies between fractal aggregates and small particles in a turbulently sheared fluid. *Environ. Sci. Technol.* 31:1237–1242.

Marguire, G. A., T. S. Edgington, and E. F. Plow. 1980. Interaction of fibrinogen with its platelet receptor as part of a multi-step reaction in ADP-induced platelet aggregation. *J. Biol. Chem.* 255:154–161.

Masliyah, J. H., G. Neale, K. Malysa, and T. G. M. van de Ven. 1987. Creeping flow over a composite sphere: solid core with porous shell. *Chem. Eng. Sci.* 42:245–253.

Mazurov, A. V., S. G. Khaspekova, T. V. Byzova, O. Y. Tikhomirov, M. C. Berndt, B. Steiner, and W. C. Kouns. 1996. Stimulation of platelet glycoprotein IIb-IIIa (alpha IIb beta 3-integrin) functional activity by a monoclonal antibody to N-terminal region of glycoprotein IIIa. *FEBS Lett.* 391:84–88.

Michalopoulou, A. C., V. N. Burganos, and A. C. Payatakes. 1991. Hydrodynamic interactions of two permeable particles moving slowly along their centerline. *Chem. Eng. Sci.* 48:2889–2900.

Pakdel, P., and S. Kim. 1991. Mobility and stresslet functions of particles with rough surfaces in viscous fluids: a numerical study. *J. Rheol.* 35:797–823.

Prieve, D. C., and E. Ruckenstein. 1976. The surface potential of and double-layer interaction force between surfaces characterized by multiple ionizable groups. *J. Theor. Biol.* 56:205–228.

Savage, B., E. Salvidar, and Z. M. Ruggeri. 1996. Initiation of platelet adhesion by arrest onto fibrinogen or translocation on von Willebrand factor. *Cell.* 84:289–297.

Schootemeijer, A., G. Gorter, L. G. J. Tertoolen, G. van Willigen, S. W. de Laat, and J. W. N. Akkerman. 1993. Lateral mobility of glycoprotein IIb/IIIa in the plasma membrane of megakaryotes. *Thromb. Haemostasis.* 69:784, 866.

Smoluchowski, M. V. 1917. Vensuch einer mathematischen theorie der koagulation kinetic kolloider losungen. *Zeitschrift fur Physikalische Chemie* 92:129–168.

Taylor, A. D., S. Neelamegham, J. D. Hellums, C. W. Smith, and S. I. Simon. 1996. Molecular dynamics of the transition from L-selectin to β_2-integrin dependent neutrophil adhesion under defined hydrodynamic shear. *Biophys. J.* 71:3488–3500.

Torres, F. E., W. B. Russel, and W. R. Schowalter. 1991. Flow structure and growth kinetics for rapid coagulation of polystyrene colloids. *J. Colloid Int. Sci.* 142:554–574.

van de Ven, T. M. 1989. Colloidal Hydrodynamics. Academic Press, London.

Wang, H., A. Z. Zinchenko, and R. H. Davis. 1994. The collision rate of small drops in linear flow fields. *J. Fluid Mech.* 265:161–188.

Weisel, J. W., C. Nagaswami, G. Vilarie, and J. S. Bennett. 1992. Examination of the platelet membrane glycoprotein IIb-IIIa complex and its interaction with fibrinogen and other ligands by electron microscopy. *J. Biol. Chem.* 263:16637–16643.

Zeichner, G. R., and W. R. Schowalter. 1977. Use of trajectory analysis to study stability of colloidal dispersion in flow fields. *AIChE J.* 23: 243–254.